Coupling of multiple LSP and SPP resonances: interactions between an elongated nanoparticle and a thin metallic film

Arash Farhang, Nicolas Bigler, and Olivier J. F. Martin*

Nanophotonics and Metrology Laboratory, Swiss Federal Institute of Technology Lausanne, EPFL-STI-NAM, Station 11, CH-1015 Lausanne, Switzerland

**Corresponding author: olivier.martin@epfl.ch*

Received June 19, 2013; revised September 17, 2013; accepted October 16, 2013; posted October 16, 2013 (Doc. ID 192615); published November 12, 2013

We study the coupling interactions between a progressively elongated silver nanoparticle and a silver film on a glass substrate. Specifically, we investigate how the coupling between localized surface plasmons (LSPs) and propagating surface plasmon polaritons (SPPs) is influenced by nanoparticle length. Although the multiple resonances supported by the nanoparticle are effectively standing wave surface plasmons, their interaction with the SPP continuum of the underlying Ag film indicates that their spectral response is still localized in nature. It is found that these LSP–SPP interactions are not limited to small particles, but that they are present as well for extremely long particles, with a transition to the SPP coupling interactions of a bilayer metallic film system beginning at a particle length of approximately 5 μm.

OCIS codes: (240.6680) Surface plasmons; (240.0240) Optics at surfaces; (250.5403) Plasmonics.
http://dx.doi.org/10.1364/OL.38.004758

Coupling of metallic nanostructures in plasmonic systems has been a topic of major research interest, as it leads to effects such as strong near-field confinement, useful for trapping, sensing, nonlinear interactions, and surface-enhanced Raman scattering [1–6]. Coupling between finite-size plasmonic nanostructures and a conductive film is of particular interest as it involves the interaction of discrete localized resonances with a continuum of delocalized surface plasmon polaritons (SPPs) [7–11]. Systems exhibiting coupling of just a few localized resonances with a delocalized continuum have already been researched [7,8]. However, the interaction between an ever-growing number of higher order localized plasmon resonances and a SPP resonance continuum has yet to be discussed. Specifically, it is well known that coupling between a localized surface plasmon (LSP) resonance and a SPP continuum leads to an observable anticrossing at the LSP resonance frequency [7,8,12–21]. What is not clear, however, is if this still holds true for a large number of localized resonances, as will be investigated in this Letter.

The system studied here consists of a 2D silver nanoparticle of 40 nm height and variable length L spaced 100 nm above a 50 nm thick Ag film on a SiO_2 substrate of refractive index $n = 1.46$ [Fig. 1(a)]. A 2D geometry was chosen since effects along the third dimension are irrelevant. We use the dielectric data for silver measured by Johnson and Christy [22]. The simulation method carried out in this study is based on Green's tensor formalism in 2D [23]. As shown in Fig. 1(a), a horizontally oriented electric dipole source placed 100 nm to the left of the particle is used for excitation. A study of the system response for a finite length L is made via the same Fourier analysis method as in a previous work [24]. The plots obtained display the magnitude of the parallel k-vector component k_x at each given frequency. Note that use of this Fourier analysis method leads to an unavoidable spectral broadening in k-space, which is inversely proportional to the particle length L, but does not pose any limitation on the current study.

The sampling points used in the Fourier analysis are taken between the Ag particle and the film. This choice allows observing the effect of the localized particle modes on the dispersion of the total system. Intuitively, we expect such coupling interactions up to a certain length L, whereas for greater lengths, the system response should converge to that of two coupled films. By solving Maxwell's equations in the limit where $L \to \infty$ and assuming TM polarization, we can calculate the eigenmodes of the asymptotic system. The calculations reveal three distinct SPP modes with dispersions shown in Fig. 1(b) and field profiles, with the E_x component depicted along the schematic in Fig. 1(a). Fourier analysis for a large length of $L = 15$ μm shows the three SPP modes, thus confirming the intuitive picture [Fig. 1(c)]. Note, the central branch corresponding to mode II is of greatest intensity, since it exhibits a close to symmetric E_x field component along the top and bottom interfaces of the particle, much like that exhibited by the many localized modes of the single elongated Ag particle in freespace [24]. The branch corresponding to mode III is of smallest intensity, since the field is most concentrated along the glass–Ag interface and thus, is excited least efficiently.

To understand the response of this system when L is much smaller, it should first be noted that the excitation of the Ag particle via a horizontally oriented dipole source in a symmetric background environment will lead to the excitation of many higher order localized modes. These modes are essentially standing wave surface plasmons and together form the continuum of the even SPP mode as $L \to \infty$ [24]. This assumption still holds for this particle–film system, since the particle is spaced 100 nm from the surface of the film. Furthermore, the use of the electric dipole source also allows the excitation of the SPP modes within the Ag film.

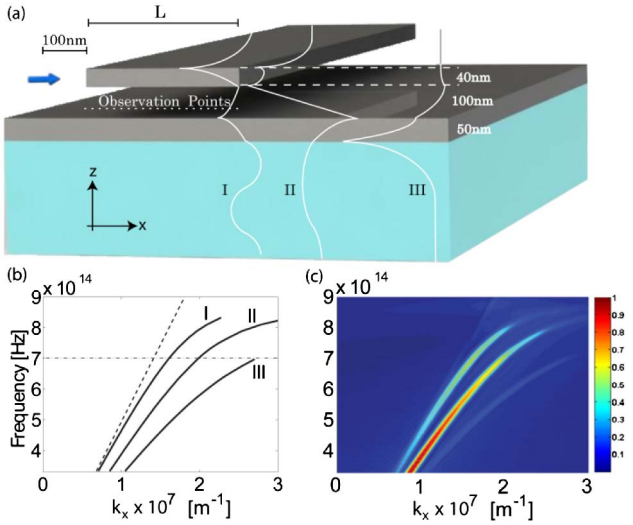

Fig. 1. (a) Silver nanoparticle of length L spaced 100 nm above a continuous silver film on glass. The system is excited by a horizontally oriented electric dipole (blue arrow). Eigenmode calculated E_x field components for the three modes I, II, and III in the limit where $L \to \infty$ are depicted along the structure. These are plotted for a frequency of 7×10^{14} and k_x values $\mathrm{I} = 1.6 \times 10^7$ m^{-1}, $\mathrm{II} = 1.972 \times 10^7$ m^{-1}, and $\mathrm{III} = 2.7 \times 10^7$ m^{-1}. (b) SPP dispersion for the three propagating modes I, II, and III in the limit of a bilayer metal film system. (c) Dispersion diagram for the Ag particle plus film system with $L = 15$ μm, showing emergence of the three propagating modes (normalized).

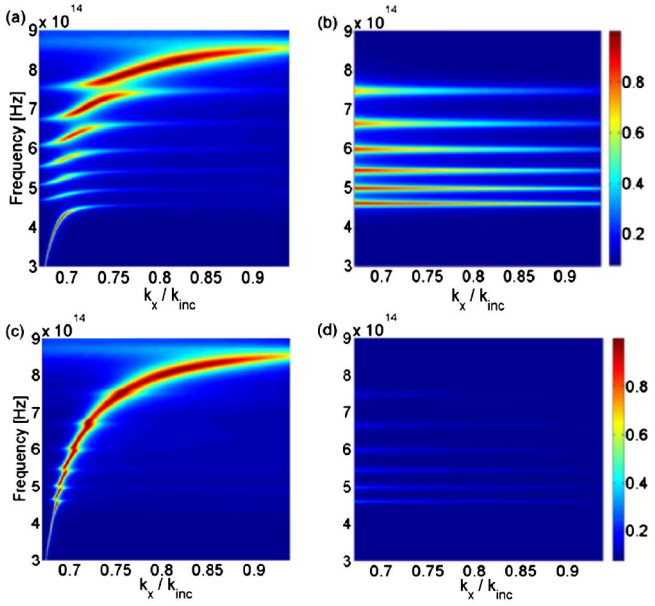

Fig. 2. Absorption plots obtained via analytical transfer matrix method calculations, showing the coupling interactions between a 50 nm Ag film on glass and an overlaying 100 nm absorbing layer with six nondispersive resonances. The x-axis indicates the ratio between the parallel k_x component and the incident k-vector magnitude k_{inc}. (a, b) Effects with strong absorption over a large range of k-vectors and (c, d) over a smaller range of k-vectors with smaller absorption.

Typically, when a single localized or nondispersive mode is coupled to a SPP continuum, a single anticrossing is seen in the dispersion [25,26] and when multiple nondispersive modes are coupled to a SPP continuum, multiple anticrossings are seen in the SPP dispersion [27]. Note, for a coupling interaction to occur, spectral and spatial overlap must be present. Given such nondispersive modes extending over a large range of k-vectors at their specific frequencies, one will also observe their coupling interaction with the SPP continuum over a large range of k-vectors [Fig. 2(a)]. If, however, each one occurs over a specific/smaller range of k-vectors, then the coupling will also occur only over that range of k-vectors [Fig. 2(c)]. The effects of coupling in these two cases can be illustrated by considering a 100 nm thick absorbing layer placed directly on top of a 50 nm Ag film on a glass substrate. Here, the absorbing layer is modeled as one with six nondispersive (fixed-frequency) resonance bands, each with a Lorentzian line shape. SPPs are excited from the glass side via p-polarized total internal reflection illumination. Calculations are made via an analytical transfer matrix formulation based simply on Fresnel coefficients [28]. First, the two different absorbing layers are considered successively and investigated in the absence of silver. For the first case [Fig. 2(b)], the resonances are designed such that they exhibit a relatively high absorption even at larger values of k_x. For the second case [Fig. 2(d)], absorption at each of the resonances is designed to be much lower and to decay to almost negligible quantities at a higher k_x. We now consider the coupled systems that include the Ag film and the absorbing layer. For the first case, we observe very distinct anticrossing line shapes in the Ag film dispersion [Fig. 2(a)], whereas for the second case, much less pronounced anticrossing line shapes are observed [Fig. 2(c)].

With the chosen Fourier analysis technique, particle lengths for which a dispersion diagram can be obtained are typically on the order of $L \geq 1$ μm. At these sizes, the LSP modes are standing wave plasmons at specific frequencies and k_x values, which together form peaks along the dispersion curve of the even SPP mode [24]. Thus, one should see a similar coupling interaction as that in Fig. 2(c).

We start the analysis with a particle of length $L = 1$ μm and compare its dispersion [right panel in Fig. 3(a)] to that of a lone particle in a freespace background [left panel in Fig. 3(a)]. Note, the additional weak ghost patterns in all plots, which become finer as L is increased, are artifacts resulting from the Fourier analysis method that disappear as $L \to \infty$. As can been seen, the dispersion maxima of the lone particle, marked with dashed lines in Fig. 3(a), correspond precisely with the dispersion minima of the particle–film system, indicating the presence of the predicted coupling interactions between the particle and the film. In fact, for the particle–film system studied here, the coupling interactions result in this observed dispersion response rather than the typical anticrossing line shapes one expects at the multiple resonances of the lone particle. This is precisely because the particle resonances exhibit a very small extent in k-space.

Furthermore, we can see from the analysis that this coupled mode is one that will converge to mode II as $L \to \infty$. The same coupling interaction is observed for a particle of length $L = 2.5$ μm [Fig. 3(b)]. Additionally,

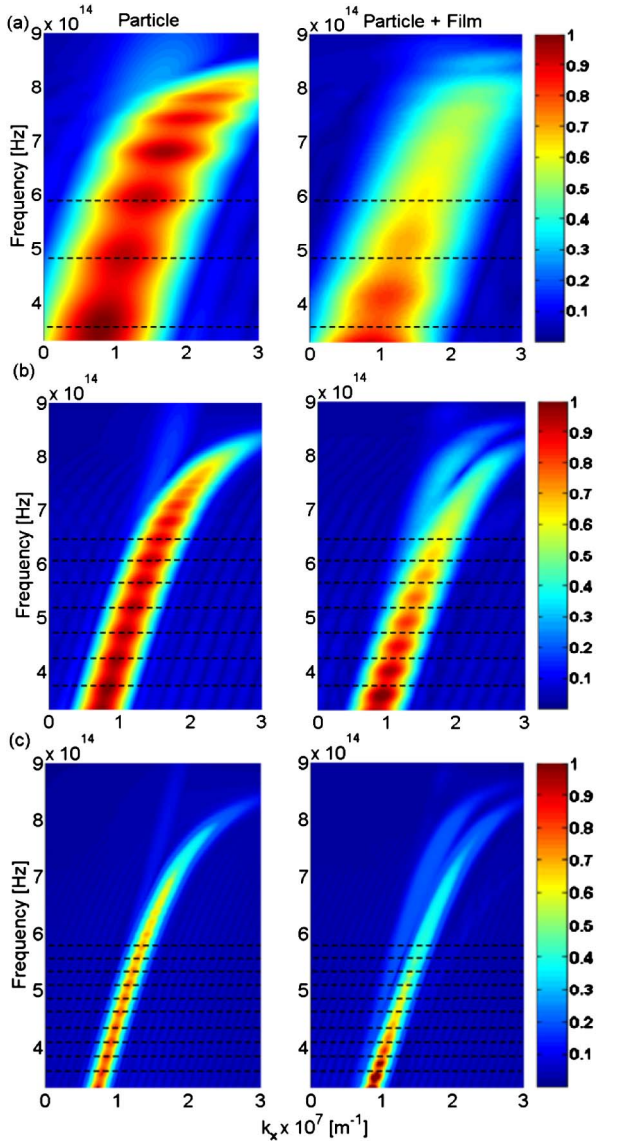

Fig. 3. Dispersions (normalized) for a Ag particle (left panels) and for the Ag particle+film system (right panels) in Fig. 1, obtained via a Fourier analysis of the near field. Results for particle lengths of (a) $L = 1$ μm, (b) $L = 2.5$ μm, and (c) $L = 5$ μm are shown. As can be seen, the minima in the dispersion curve of the total system correspond with the maxima in the dispersion of the lone particle, indicating the presence of LSP–SPP coupling interactions between the particle resonances and the SPP continuum of the film.

at this length, the upper tail of another SPP curve becomes visible due to a decrease in spectral broadening. This mode corresponds to mode I for the $L \to \infty$ system (Fig. 1). Notice that coupling between the many localized modes of the particle and the SPP continuum of the film occurs only for mode II. This is simply due to the fact that in this case, SPPs are bound to both interfaces of the top Ag film, and that they exhibit a close to symmetric E_x field profile in the top Ag film, just like that exhibited by the many localized modes of the single elongated Ag particle in freespace [24]. Note, however, that we do not expect the field E_x to be completely symmetric in the top film, since the total environment itself is not symmetric. For a length of $L = 5$ μm [Fig. 3(c)], the transition to a bimetallic film system becomes apparent. For frequencies below approximately 450 THz, dips/anticrossings in the SPP dispersion of the particle–film system continually match up with the resonance peaks of the lone particle, whereas at frequencies above 450 THz, where the single SPP curve splits into not just two, but three branches, these are lost. At $L = 15$ μm, as shown in Fig. 1(c), the splitting of the single SPP curve into three branches becomes much more distinct. This, in addition to the fading of LSP–SPP anticrossings and the formation of a SPP continuum, indicates that coupling between localized and propagating modes is not limited by the number of localized modes interacting with the continuum, but rather whether the particle has become sufficiently long to support freely propagating plasmons and thus, has entered the coupling realm of a bilayer film system.

In conclusion, we have studied the coupling between a progressively elongated Ag nanoparticle and a Ag film on a glass substrate. We have demonstrated that the coupling between the two leads to the typically observed spectral dips/anticrossings at every single one of the particle's resonances. This characteristic form of localized and delocalized (LSP–SPP) plasmon coupling is present for any particle length, right up to the limit where the particle becomes long enough to support freely propagating plasmons rather than localized standing wave plasmons [24] and thus enters the coupling realm of two metallic films. Such findings may be of relevance for systems with short metallic sections, examples being coupled-line bandpass filters implemented in the optical regime and also systems exhibiting gap-plasmon resonances [29,30].

Funding from the State Secretariat for Education and Research SER within the Indo Swiss Joint Research Programme and the Swiss National Science Foundation (project 200021-125326) is gratefully acknowledged.

References

1. J. N. Anker, W. P. Hall, O. Lyandres, N. C. Shah, J. Zhao, and R. P. Van Duyne, Nat. Mater. **7**, 442 (2008).
2. B. Sepulveda, P. C. Angelome, L. M. Lechuga, and L. M. Liz-Marzan, Nano Today **4**(3), 244 (2009).
3. W. Zhang, H. Fischer, T. Schmid, R. Zenobi, and O. J. F. Martin, J. Phys. Chem. C **113**, 14672 (2009).
4. D.-K. Lim, K.-S. Jeon, J.-H. Hwang, H. Kim, S. Kwon, Y. D. Suh, and J.-M. Nam, Nat. Nanotechnol. **6**, 452 (2011).
5. M. Kauranen and A. V. Zayats, Nat. Photonics **6**, 737 (2012).
6. K. Thyagarajan, S. Rivier, A. Lovera, and O. J. F. Martin, Opt. Express **20**, 12860 (2012).
7. P. Nordlander and E. Prodan, Nano Lett. **4**, 2209 (2004).
8. F. Le, N. Z. Lwin, N. J. Halas, and P. Nordlander, Phys. Rev. B **76**, 165410 (2007).
9. W. L. Barnes, A. Dereux, and T. W. Ebbesen, Nature **424**, 824 (2003).
10. T. Sondergaard and S. I. Bozhevolnyi, Phys. Rev. B **69**, 045422 (2004).
11. A. V. Zayats, I. I. Smolyaninov, and A. A. Maradudin, Phys. Rep. **408**, 131 (2005).
12. W. R. Holland and D. G. Hall, Phys. Rev. B **27**, 7765 (1983).
13. J. Cesario, R. Quidant, G. Badenes, and S. Enoch, Opt. Lett. **30**, 3404 (2005).
14. G. Lévêque and O. J. F. Martin, Opt. Express **14**, 9971 (2006).
15. N. Papanikolaou, Phys. Rev. B **75**, 235426 (2007).

16. J. Cesario, M. U. Gonzalez, S. Cheylan, W. L. Barnes, S. Enoch, and R. Quidant, Opt. Express **15**, 10533 (2007).
17. A. Christ, G. Lévêque, O. J. F. Martin, T. Zentgraf, J. Kuhl, C. Bauer, H. Giessen, and S. G. Tikhodeev, J. Microsc. **229**, 344 (2008).
18. G. Lévêque and R. Quidant, Opt. Express **16**, 22029 (2008).
19. Y. Chu and K. B. Crozier, Opt. Lett. **34**, 244 (2009).
20. D. Brunazzo, E. Descrovi, and O. J. F. Martin, Opt. Lett. **34**, 1405 (2009).
21. J. DiMaria and R. Paiella, J. Appl. Phys. **111**, 103102 (2012).
22. P. B. Johnson and R. W. Christy, Phys. Rev. B **6**, 4370 (1972).
23. M. Paulus and O. J. F. Martin, Phys. Rev. E **63**, 066615 (2001).
24. A. Farhang and O. J. F. Martin, Opt. Express **19**, 11387 (2011).
25. A. Ghoshal and P. G. Kik, J. Appl. Phys. **103**, 113111 (2008).
26. A. Ghoshal, I. Divliansky, and P. G. Kik, Appl. Phys. Lett. **94**, 171108 (2009).
27. S. Dutta-Gupta and O. J. F. Martin, J. Appl. Phys. **110**, 044701 (2011).
28. B. E. A. Saleh and M. C. Teich, "Guided-wave optics," in *Fundamentals of Photonics* (Wiley, 2001), pp. 238–271.
29. D. Pozar, *Microwave Engineering* (Wiley, 1997).
30. J. Jung, T. Sondergaard, and S. I. Bozhevolnyi, Phys. Rev. B **79**, 8 (2009).